Mechanism of the Electronic Stabilization of the 3MR and Divalent Carbon of Bis(diisopropylamino)cyclopropenylidene

Lucius E. Johnson and Donald B. DuPré*

Department of Chemistry, University of Louisville, Louisville, Kentucky 40292

Received: March 5, 2007; In Final Form: July 16, 2007

Analysis of the topology of the electron density of bis(dimethylamino)cyclopropenylidene as a model of the recently synthesized, stable bis(diisopropylamino)cyclopropenylidene with the quantum theory of atoms in molecules is used to investigate the stabilizing electronic effects at the reactive carbene site by amino substitution. This work demonstrates that the plane perpendicular lone pairs of nitrogen utilize in-plane σ-aromaticity as a conduit to delocalize charge to the carbene carbon C2, where it is transferred preferentially back into the π-plane at the site through $\sigma-\pi$ polarization. C2 is thus stabilized relative to the parent cyclopropenylidene, c-C_3H_2, by a very different mechanism than that suggested in the orbital view of n_π(N) and π(C═C) conjugation and n_π(N) → p_π*(C2) hyperconjugation. Validation of this premise is also found in properties of asymmetric atomic quadrupole tensors, bond path ellipticities, and diamagnetic/paramagnetic components of NMR shielding tensors.

I. Introduction

Cyclopropenylidene, c-C_3H_2 (**1** of Scheme 1), is the smallest aromatic carbene. The compound, although highly reactive, has been detected spectroscopically by radio astronomy[1,2] in significant abundance in outer space and by matrix isolation procedures[3] and in low-density plasmas[1,4−6] in the laboratory. The molecule has a large dipole moment that enhances its spectroscopic visibility in the laboratory and interstellar molecular clouds.[7] Linear chain isomers of c-C_3H_2 have also been observed,[2,3,8−10] as well as ring-substituted analogues with, for example, R = Cl [11], F [12], and phenyl.[13,14] After having synthesized a remarkable series of stable carbenes,[15,16] Bertrand's group[17] recently achieved the isolation and obtained the crystal structure of the amino-substituted bis(diisopropylamino)-cyclopropenylidene (**3**) with R = N(*i*-Pr)$_2$. The authors invoked π-type aromaticity to account for the electronic stabilization of the compound as depicted in Scheme 1. This result is unusual as the nitrogen π-donors are two bonds removed from, rather than right next to, the site of electron deficiency. The bulky isopropyl groups, of course, also sterically protect the reactive center from nucleophilic or electrophilic attack but have little effect on the electronic properties of the cyclopropenylidene ring. Stable carbenes are beginning to show great utility in various catalytic roles, such as organic synthesis,[18−21] polymerization,[22] and hydrogen and ammonia activation.[23] The investigation of the electronic structure and stability of these compounds is crucial in understanding, developing, and tuning their catalytic and chemical activity. The present work presents an alternative point of view of the electronic mechanism of cyclopropenylidene stabilization brought about through a study of the features of the topology of the electron density. It is based on the quantum theory of atoms in molecules (QTAIM),[24,25] particularly the seminal work on carbenes by MacDougall and Bader.[26] The sources of stabilization or destabilization of atoms in the cyclopropenylidene ring by amino substitution, relative to the R = H parent compound, can be traced to three physical factors: (i) charge transfer, which redistributes electron density from the atomic basins of more electropositive elements to those of more electronegative elements; (ii) σ-aromaticity[27−30] [a three-membered ring (3MR) effect] that redistributes and preferentially concentrates electron density in the surface of the ring; and (iii) filling in of the C2 p_π* voids (cf., Scheme 1 for the orbital counterpart) through $\sigma-\pi$ polarization[31−33] (not π-back-donation), which pushes in-plane charge into regions (gaps) of charge depletion perpendicular to the molecular plane. The physical and chemical significance of these factors will be elaborated below.

II. Methods

The equilibrium geometries of the molecules of this study were fully optimized, and normal-mode frequency analysis was performed, using density functional theory (DFT) at B3LYP/6-31G(d,p),[34,35] as implemented in Gaussian03.[36] Larger basis sets were investigated but produced no improvement in the geometric parameters as compared to the available experimental values. The coordinates of all optimized models of this study are found in the Supporting Information for this paper.

The resultant electron density, ρ, obtained from the wave function of all optimized structures, was analyzed with the quantum theory of atoms in molecules (QTAIM)[24,25] using the AIM2000 program[37] with wave functions generated with Gaussian03.[36] According to QTAIM, an atom in a molecule is rigorously defined as a quantum mechanical entity bounded by a three-dimensional surface of zero flux in the gradient, $\nabla\rho$, of the electron density ρ ($\nabla\rho(r)\cdot\mathbf{n}(r) = 0$ for all points r on the atomic boundary, where $\mathbf{n}(r)$ is a unit vector normal to the surface at a point r). Given this delineation of the boundaries of an atom, the net charge, dipole, quadrupole, and degree of electron localization/delocalization of an individual atom can be obtained by integration of moments of the electron density over the atomic volume (referred to as the atomic basin). Little change was found in the QTAIM properties calculated, at a much higher computational cost, with basis sets more extended

* To whom correspondence should be addressed. E-mail: d.dupre@louisville.edu.

10.1021/jp0717894 CCC: $37.00
Published on Web 10/11/2007

SCHEME 1

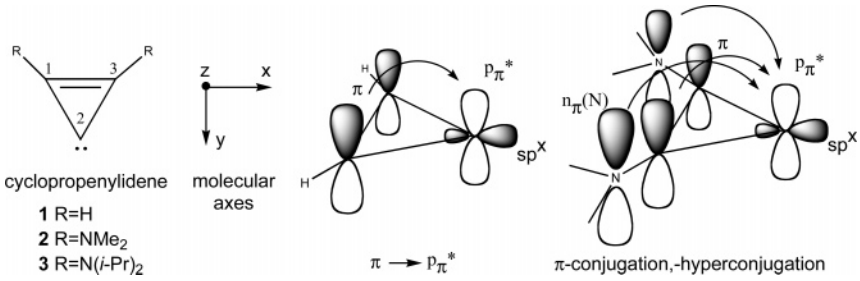

than 6-31G(d,p). It is assumed that the reader is familiar with the QTAIM. The following therefore will serve to merely define symbols used in this article. A more complete discussion of QTAIM is found in the Supporting Information.

The bond critical point (BCP) is a (3, −1) critical point (CP) of ρ on the bond path (BP) and interatomic surface (IAS) adjoining two atoms. A ring critical point (RCP) is a (3, +1) CP of ρ of a molecule with a closed surface. The Laplacian, $\nabla^2\rho_b$, at a BCP may be written in terms of the eigenvalues of the Hesssian of ρ as $\nabla^2\rho = \lambda_1 + \lambda_2 + \lambda_3$, where $\lambda_1 \leq \lambda_2 \leq \lambda_3$. The ellipticity of the axial curvature of ρ about the BP is defined as $\epsilon = (\lambda_1/\lambda_2) - 1$. CPs of the Laplacian uncover regions of valence shell charge concentration (VSCC), denoted by (3, −3) CPs, and regions of charge depletion that may breach the band of VSCC, characterized by (3, +1) CPs. The degree of localization, λ(A), of electrons within a QTAIM-defined atomic basin, A, and their delocalization, δ(A,B), into the basin of another atom, B, were also calculated as described by Fradera et al.[38] and Biegler-Konig and Schonbohm.[37]

^{13}C NMR shielding tensors, σ, were obtained with the gauge-including atomic orbital (GIAO)[39,40] method at the B3LYP/6-31G(d,p) level of theory. This method has been shown to produce reliable results in shielding calculations,[41−43] while providing here a consistent level of theory for comparison with the QTAIM-calculated properties. The principal components of the tensors, σ_{xx}, σ_{yy}, and σ_{zz}, are the results of an applied magnetic field in the *x*-, *y*-, or *z*-direction, respectively. Our calculations included the direction cosines and the diamagnetic and paramagnetic contributions, σ^d and σ^p, respectively, of the isotropic value $\sigma_{iso} = (\sigma_{xx} + \sigma_{yy} + \sigma_{zz})/3$ of the tensors. Chemical shifts were obtained with reference to TMS using the isotropic value of $\sigma(^{13}C; TMS) = 191.8$ ppm calculated at the same level of theory. Plots of the shielding density isosurfaces were created in gOpenMol[44,45] using cube files generated with the cubegen utility in Gaussian03.[36]

III. Results and Discussion

1. Geometric Parameters and Ring Strain. The geometric parameters of the optimized structures of the cyclopropenylidenes, Scheme 1, of this study are shown in Table 1. Bis(dimethylamino)cyclopropenylidene, **2**, was determined to be a suitable model for the synthesized bis(diisopropylamino)-cyclopropenylidene, **3**. The calculated bond distances, R_e, and straight-line bond angles, α_e, of **2**, where R = NMe_2, agree well with the experimental values obtained from the crystal structure[17] of **3**, where R = N(*i*-Pr)$_2$. Initial comparison of calculated QTAIM properties of **3** and the abbreviated model **2** showed little difference as well. Integration of the atoms of **3**, however, proved to be much more computationally expensive. No BP and very slight electron delocalizations were found between the sterically blocking isopropyl groups and the ring carbons—consequently, their effect on the electronic stability of the system is minimal. The calculated bond distances and bond angles for the R = H analogue, **1**, also agree well with experimental data obtained from rotational spectra.[6] The equilibrium bond length (straight-line internuclear distance, R_e) of the short C1═C3 bond is indicative of double bond character. The long bonds to C2 are shorter than usual carbon−carbon single bonds even in molecules with 3MRs and other carbon bonds to divalent carbon—examples being cyclopropane and the singlet $(CH_3)_2C$ carbene, where the calculated values of R_e(C−C) are 1.508 and 1.477 Å, respectively. The topological properties of the BPs between carbon atoms reveal considerable ring strain. As shown in Figure 1, the BPs with path lengths R_b curve outward and thus deviate from the value of R_e. This is shown in the table with values of $\Delta R = R_b - R_e$[31,46] and the index $Q = (R_b/R_e - 1) \times 1000$ proposed by Cremer and Kraka[29] that better accentuates the difference. Thus, to partially overcome the effects of ring strain, the charge density in the σ-plane is found to relax and the BPs curve outward.[46] The angles, α_b, tangential to the curved BPs at the carbon nuclei, also deviate from the straight-line bond angles. Strain relaxation[31,46] is particularly evident in α_b at the C1 and C3 carbons ($\alpha_b = 82.6$ and 85.1° for R = H and R = NMe_2, respectively), and the outward curvature of the BP is greatest for the C1═C3 bond. The corresponding angles at the C2 nucleus are more acute ($\alpha_b = 63.2°$ for both cases), and the deviations $\Delta\alpha$ are less. Finally, the calculated value of the molecular dipole of cyclopropenylidene (R = H) of 3.20 D agrees well with the experimental value of 3.43 D determined by microwave spectroscopy.[7] It is

TABLE 1: Geometric Parameters of Cyclopropenylidenes (R = H, NMe_2) Optimized at B3LYP/6-31G(d,p)[a]

				experimental[e]	experimental[c]
	R =	H	NMe_2	H	N(*i*-Pr)$_2$
C═C	R_e	1.325	1.354	1.320	1.344
	R_b	1.338	1.371		
	ΔR	0.013	0.017		
	Q	9.8	12.6		
C−C	R_e	1.430	1.414	1.417	1.405
	R_b	1.435	1.421		
	ΔR	0.005	0.007		
	Q	3.5	5.0		
C−R[b]	R_e	1.082	1.347	1.075	1.336
∠C1C2C3	α_e	55.2	57.2	55.5	57.2
	α_b	63.2	63.2		
	$\Delta\alpha$	8.0	6.0		
∠C1C3C2	α_e	62.4	61.4	62.2	61.4
	α_b	82.6	85.1		
	$\Delta\alpha$	20.2	23.7		
μ(D)		3.20		3.43[d]	

[a] Equilibrium molecular bond lengths (R_e) and BP distances (R_b) of the topological molecular graph in Å; molecular bond angles (α_e) and BP angles (α_b) at central atoms in degrees. $\Delta R = R_b - R_e$, $\Delta\alpha = \alpha_b - \alpha_e$, $Q = (R_b/R_e - 1) \times 1000$. [b] First atom of R group. [c] Ref 17. [d] Experimental value of molecular dipole in Debye from ref 7. [e] Experimental geometric parameters from rotational spectra; ref 6.

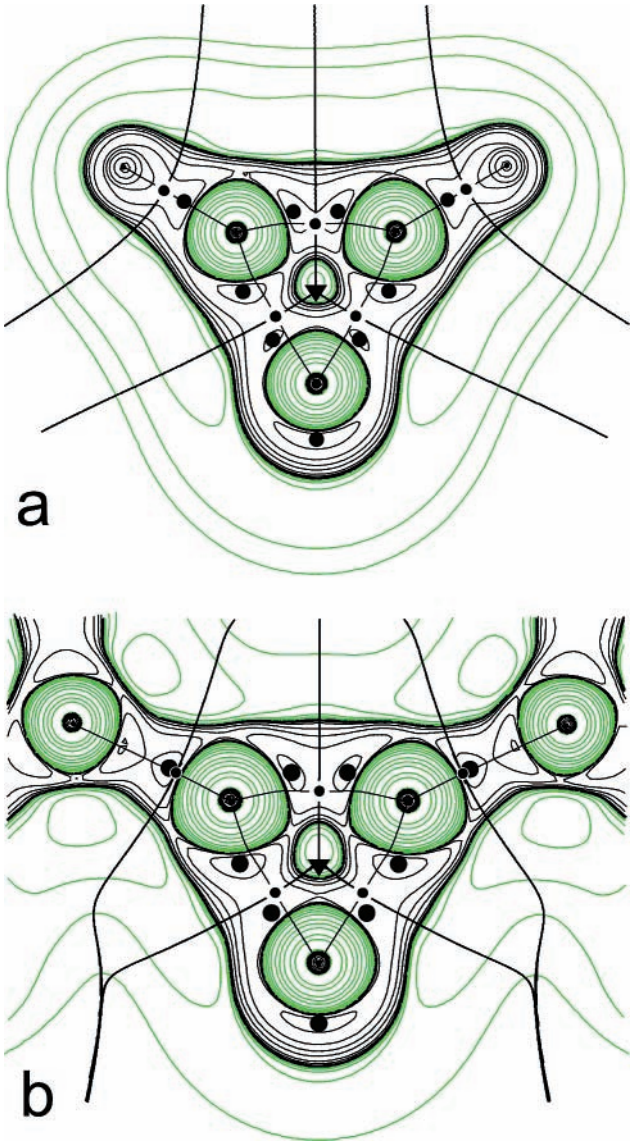

Figure 1. Overlay of BPs (thin dark lines connecting nuclear centers), lines (thicker) where the IASs cut the plane of the molecule and contour plots of the Laplacian of the electron density for (a) R = H and (b) R = NMe_2. Dark lines in the Laplacian plot delineate regions of charge concentration; green lines map regions of charge depletion. Small dark circles on the IASs and BPs locate (3, −1) BCPs. The larger circles are bonded or nonbonded (3, −3) CPs in the valence shell. The triangles are the (3, +1) RCPs. The plots are not to scale. C2 is the lower atomic basin in both plots with an outwardly pointed nonbonded charge concentration.

this large molecular dipole that allows the spectroscopic detection of c-C_3H_2 in outer space.

2. Stabilization of the Reactive Divalent Carbon of Substituted Ylidenes. QTAIM Atomic Energies and Populations. The QTAIM integrated atomic energies (Table 2) show that C2 is stabilized relative to R = H by substitution with R = NMe_2 where $\Delta E = -24.7$ kcal/mol, while C1 and C3 are destabilized, with $\Delta E = 154.7$ kcal/mol. These results correlate with the integrated atomic populations. The almost neutral charge on C2 for the R = NMe_2 case is indicative of an operative push−pull effect of the planar nitrogens across *two* bonds. That is, even though nitrogen is more electron withdrawing, there are more electrons, N(A), in the atomic basin of C2 when R = NMe_2 ($N = 6.02$) than when R = H ($N = 5.91$). With more electrons, nitrogen will obviously have more interaction with the ring carbons than hydrogen, even across

TABLE 2: Calculated QTAIM Atomic Properties of Cyclopropenylidene Series: Atomic Charges, Atomic Energy (E), Atomic Virial ($\mathcal{V}$), Localization λ(C2)/Delocalization δ(C2) Indices of C2, and Other Atomic Properties of C2 and C1(C3) Including Atomic Population (N) and Stabilization/Destabilization Energy (ΔE) Relative to R = H

R =	H	NMe_2
atomic charges (e)		
C1, C3	−0.1314, −0.1319	0.3724, 0.3724
C2	0.0902	−0.0201
H, N	0.0884, 0.0897	−1.1909, −1.1913
C2 properties		
N(C2)	5.91	6.02
E(C2) (au)[a]	−37.880988	−37.920380
ΔE (kcal/mol)	0	−24.7
virial ratio, γ	2.009254	2.009689
K (au)[b]	37.53366	37.55648
atomic virial $\mathcal{V}'$ (C2)[c]	−75.0692	−75.1118
basin virial $\mathcal{V}'_b$(C2)	−75.0099	−75.0532
surface virial $\mathcal{V}'_s$(C2)	−0.0593	−0.0586
λ(C2)	4.580	4.566
δ(C2,X) with X =		
C1 (or C3)	1.279	1.260
H, N	0.050	0.124
C1 (C3) properties		
N(C1,3)	6.13	5.63
E(C1,3) (au)	−38.147104	−37.900586
ΔE (kcal/mol)	0	154.7
λ(C1)	4.141	3.620
δ(C1,Y) with Y =		
C3	1.693	1.382
H, N	0.942	1.100
H, N (C3)	0.063	0.119

[a] $E(A) = K(1 - \gamma)$, where $\gamma = -V/T$ is the virial ratio (ideally 2.0) for the whole molecule. [b] K = integrated Hamiltonian kinetic energy over atomic basin. [c] K(C2) not exactly equal to $-\mathcal{V}'/2$ due to integration error.

two bonds. The increased electron pairing between the ring carbon basins and nitrogen is evident in the delocalization indices in Table 2. To offset the loss of charge in the C1 and C3 basins, the delocalization of electrons from nitrogen helps to stabilize the system and the reactive C2 carbon as it increases from δ(C2,H) = 0.050 electrons to δ(C2,N) = 0.124 electrons. As seen in the data of Table 2, the majority of stabilization of the atom comes from $\mathcal{V}'_b$, the electronic potential energy density within the basin, which is dominated by the attraction of the electrons within the basin of C2 to the C2 nucleus. When R = NMe_2, the basin virial $\mathcal{V}'_b$(C2) = −75.0532 as compared to −75.0099 for R = H due to the higher electrostatic potential between the greater electron density and the nuclei. $\mathcal{V}'_s$, the virial of the Ehrenfest force over the surface of C2, shows very little change, indicating that R substitution has a minimal effect on the stabilization that stems from bond, and thus surface, formation of C2 with C1 and C3, even though the bond length is shorter.

3. Stabilization of the 3MR by Surface Electron Delocalization (σ-Aromaticity). As we will show now, the out-of-plane, lone pair concentrations of the planar nitrogen centers participate, preferentially, in *in-plane* σ-aromaticity—thus delivering charge to the basin of C2 by a very different mechanism than that suggested in Scheme 1.

As discussed by Bader et al.[24,46] for cyclopropane, the origin of surface delocalization (σ-aromaticity) in the 3MR structures of the sort of this study is in the interaction of the (3, −1) BCPs of the carbon−carbon bonds with the (3, +1) RCP. In all cases, the eigenvectors corresponding to the positive eigenvalues (λ_r2, λ_r3) of the Laplacian at the RCP lie in the molecular plane,

TABLE 3: Topological Properties (in au) of the BCPs of the Long and Short C−C Bonds and the RCP of Cyclopropenylidenes[a]

	R =	H	NMe_2
C═C (short bond)	ρ	0.3320	0.3031
	$\nabla^2\rho$	−0.7868	−0.6020
	$\lambda 1$	−0.5559 ⊥	−0.4860 ⊥
	$\lambda 2$	−0.5018	−0.4133
	$\lambda 3$	0.2710	0.2973
	ϵ	0.11	0.18
C−C (long bond)	ρ	0.2805	0.2867
	$\nabla^2\rho$	−0.5416	−0.5796
	$\lambda 1$	−0.5178 ⊥	−0.4965 ⊥
	$\lambda 2$	−0.3242	−0.3584
	$\lambda 3$	0.3004	0.2753
	ϵ	0.60	0.39
RCP	ρ	0.2516	0.2481
	$\nabla^2\rho$	0.1556	0.2272
	$\lambda_r 1$	−0.3749 ⊥	−0.3325 ⊥
	$\lambda_r 2$	0.2636	0.2341
	$\lambda_r 3$	0.2668	0.3256
$\eta = (\rho_r/\bar{\rho}_b) \times 100$[b]		84.5	84.9

[a] The major axis ($\lambda 2$) of the ellipticity (ϵ) of ρ and the eigenvectors of the listed eigenvalues are parallel to the molecular plane unless otherwise noted as being perpendicular (⊥) to the plane. [b] $\rho_r = \rho$(RCP), $\bar{\rho}_b$ = average value of ρ at the BCPs of the three ring carbon−carbon bonds.

whereas that of the negative eigenvalue ($\lambda_r 1$) is perpendicular to the plane. As seen in Table 3, the value of the electron density at the RCP of each molecule is comparable to those of the nearby BCPs of the ring bonds, where one of the principal axes of negative curvature also lies in the plane and points toward the ring center. The values in Table 3 of the ratio[29] $\eta = (\rho_r/\bar{\rho}_b) \times 100$ show that the minimum of the electron density, ρ_r, in the ring plane (at the RCP) amounts to 84−85% of the average of the density, $\bar{\rho}_b$, at the BCPs of the three ring carbon−carbon bonds. Because of the close proximity of these CPs and similarity of the value of the electron density, curvatures of opposite sign interact significantly with one another leading to a flattening out of the charge distribution in the ring plane. Thus, the major $\lambda 2$ eigenvector corresponding to minimum negative curvature at each BCP lies *in the ring plane*. The value of the ellipticity, $\epsilon = (\lambda 1/\lambda 2) - 1$, at the BCP is 0.60 for the long bond when R = H but falls to $\epsilon = 0.39$ when R = NMe_2 (Table 3). The ellipticity at the BCP of the short bond, however, is unusually low for a double bond, with $\epsilon \sim 0.11-0.18$, but the major axis is still *in the plane*. This is also a result of the interaction of the in-plane eigenvector, of negative eigenvalue, of the double bond BCP with the in-plane eigenvector, of positive eigenvalue, of the RCP. In both cases, electron density is crowded within the ring in the σ-plane and is the origin of ring strain seen in the compensatory, outward curvature of the BPs around the ring to relieve electron−electron repulsion. Some relief also occurs in the zone of charge depletion at the RCP near the ring center (cf. Figure 1) and in the concomitant escape of charge inside the ring, evident above and below the ring surface (cf. Figure 2) along the direction of the only negative eigenvector $\lambda_r 1$ corresponding to charge concentration. Overall, in both cases studied, the Laplacian at the RCP is positive since $\lambda_r 2$ and $\lambda_r 3$ dominate $\lambda_r 1$; that is, $|\lambda_r 2 + \lambda_r 3| > \lambda_r 1$.

For like atoms, the value of ϵ at the BCP is a good measure of the ellipticity of the whole bond.[47,48] However, the use of this parameter for unlike atoms, particularly those with substantially different electronegativities, could be misleading, and more thorough mapping[49,50] is needed of the possible change of orientation along the BP of the two eigenvectors, with

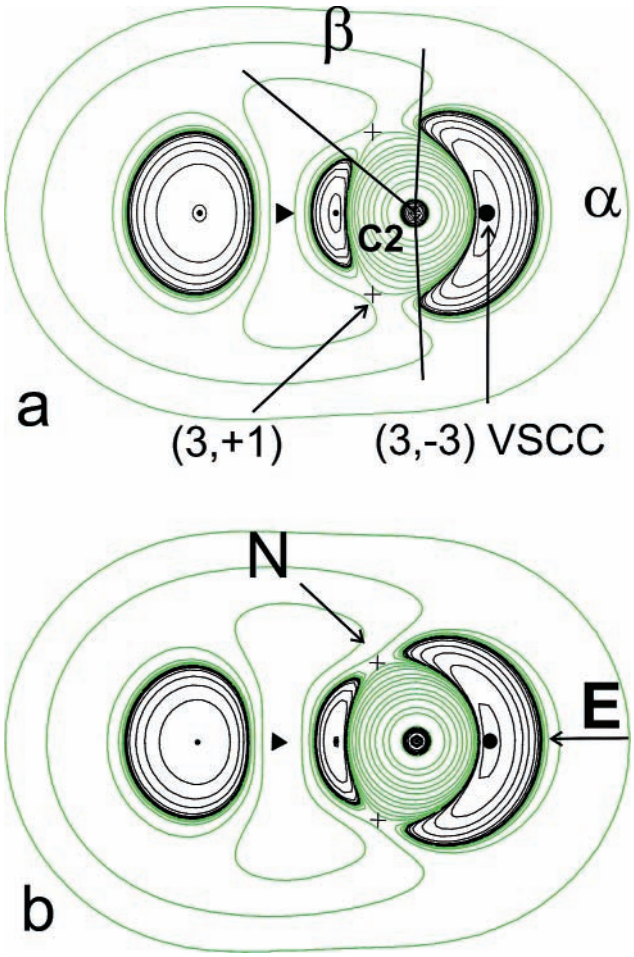

Figure 2. Perpendicular view of the contour plots of the Laplacian of the electron density in the plane bisecting the ∠C1C2C3 bond angle and passing through the center point of the C1═C3 short bond for (a) R = H and (b) R = NMe_2. The crosses locate two (3, +1) depletion CPs of C2 above and below the molecular plane. Two angles are defined as follows: the lone pair extension angle α and the valence depletion angle β. The arrows labeled **N** and **E** show preferred paths of vulnerability to nucleophilic and electrophilic attack, respectively. See the caption of Figure 1 for a description of the other features of these plots.

eigenvalues λ_1 and λ_2, associated with axial curvature of ρ about the BP. Further detail of the ellipticity along the BPs is shown in Figure 3. The major $\lambda 2$ eigenvector of the electron density along the nitrogen to ring carbon path shifts from the perpendicular plane into the molecular plane near the BCP, and it remains in the plane throughout the ring BPs. This indicates that the push−pull effect of nitrogen and the interactions of the lone pairs with the cyclopropenylidene ring occur through the mechanism of *in-plane* σ-aromaticity, rather than perpendicular plane π-conjugation.

4. Origin of Ambiphilicity of C2. The chemical activity of a singlet carbene resides in its ambiphilic nature—the ability to act as both a nucleophile and an electrophile. This is evident in the topology of the electron density about the carbon center, as seen in Figure 2. The Laplacian profiles (in the plane perpendicular to the molecular plane, bisecting the ∠C1C2C3 angle) show a region of VSCC at C2 with a nonbonding (3, −3) CP pointing away from the ring (resembling an outward-pointing "mushroom cap"), along with two regions, above and below the molecular plane, of charge depletion. Each of the latter gaps (regions of minimal VSCC—therefore, relative charge depletion) is characterized by a (3, +1) CP located by a cross. Two angles, α and β, are also defined in Figure 2a. The angle α is a measure

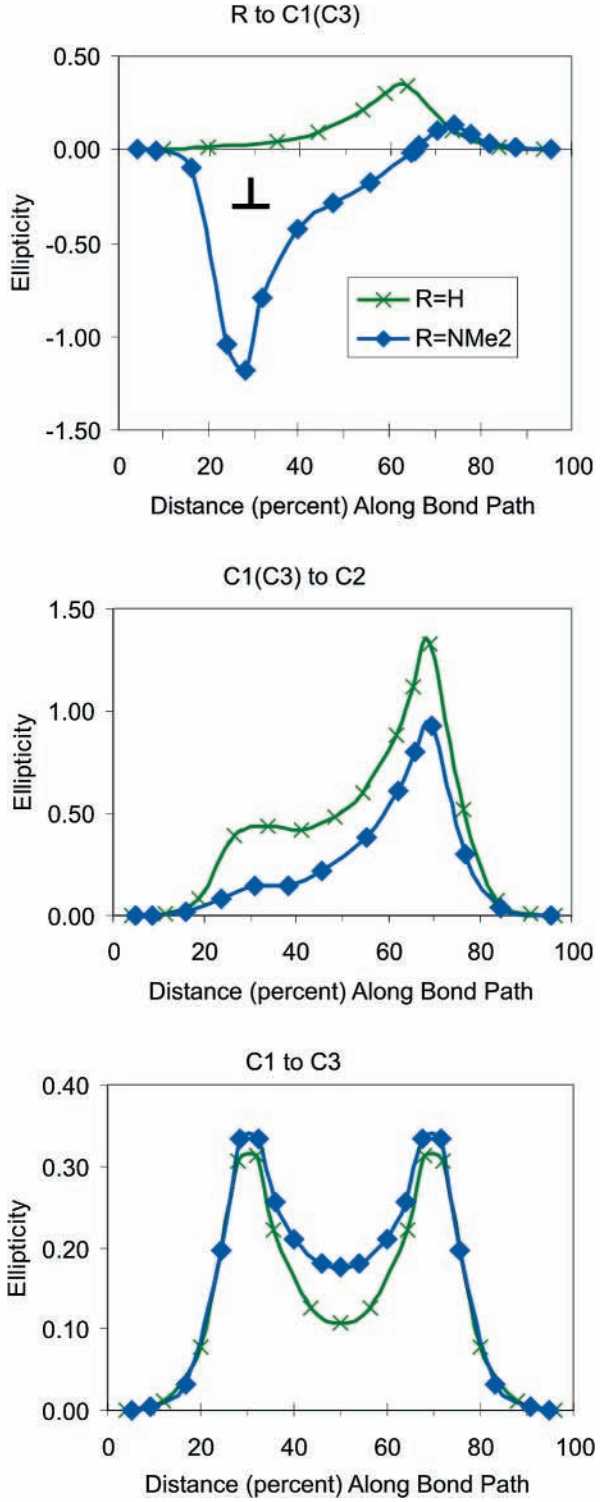

Figure 3. Graphs of the ellipticity of the electron density, as defined in the text, along the BPs. Positive values refer to points where the major axis, $\lambda 2$, is oriented in the plane of the molecule, and negative values refer to where it is perpendicular to the plane. The effects of σ-aromaticity and the preferential accumulation of charge in the plane can be traced. Even along the N−C1(C3) BP, the major axis shifts into the molecular plane.

of the extent of π-polarization of this lone pair-like concentration; β is a rough measure of the exposure of the ambiphilic C2 nucleus to nucleophilic attack.

With nitrogen substitution, charge is transferred from the ring carbons to the more electronegative nitrogens through induction. The subsequent back-polarization[24,26] of electron density drives charge into the BPs of the long and short carbon−carbon bonds of the 3MR—more so for the long bond. The latter is seen in the increased value of ρ at the BCPs of the long bonds shown in Table 3. Correspondingly, this "back-bifurcation" of charge into the carbon−carbon ring bonds results in more relative depletion of charge in the center of the ring. This is a compensatory effect that is necessary to maintain the zero-flux condition $[\nabla\rho(r)\cdot\mathbf{n}(r) = 0]$ of the atomic basins and to prevent an abnormal rise in the energy of the C1(C3) carbon atoms.[24] It is manifested in the values, found in Table 3, for ρ_r and $\nabla^2\rho_r$ at the (3, +1) RCPs, which are lower and higher, respectively, for the R = NMe_2 case. Charge is also pushed out of plane near the short bond as seen in the closing of the depletion gaps above and below C1(C3). The origin of these gaps appears to be the ring strain of the 3MR, as they are not present in the carbon atoms of ethene. As shown above in section 3, as charge is pushed into the C2 basin via the C−C long bonds, it is preferentially distributed in the σ-plane, not in the perpendicular π-plane. This, in turn, results in polarization of charge out of plane at the C2 center and a partial filling-in of the depletion gaps in the VSCC. The value of $\mu 2$, a measure of the axial thickness of the cap perpendicular to the molecular plane, mirrors the change in α and is indicative of a greater filling-in of electron density in the π-plane by the effects of the nitrogen atoms. The higher π-plane concentration is also seen in the perpendicular quadrupole component of C2 where $Q_{zz} = -0.63$ vs $Q_{zz} = -0.02$ for R = H. (The eigenvectors of the quadrupole tensor provide directions of polarization of the electron density within the atomic basin, with negative and positive eigenvalues corresponding to directions of accumulations and depletions, respectively.[51]) The resultant decrease in the β angle of depletion, as shown in Figure 2b, provides for greater stability of the molecule in the R = NMe_2 case by reducing its exposure to nucleophilic attack at the reactive carbene site. (In the synthesized compound **3**, there are of course also considerable steric restrictions to the approach of a nucleophile not accounted for in the electronic considerations of this work.)

Values of ρ and $\nabla^2\rho$ at the nonbonding (3, −3) CP of C2 vary little (see Table 4), indicating that there should be little

TABLE 4: Properties of the C2 Lone Pair and Formally Empty p_π* Orbitals along with Parameters of the VSCC and (3, +1) Valence Depletion CPs about C2 from QTAIM Topological Analysis[a]

R =	H	NMe_2
hybridization of C2[b]		
sp^x(C2)	0.56	0.66
occupancy	1.99	1.96
p_π* occupancy	0.408	0.595
VSCC[c]		
ρ	0.3018	0.2871
$\nabla^2\rho$	−1.1814	−1.0442
$\mu 3$[d]	−14.76	−13.31
$\mu 2$[e]	−0.7204	−0.5440
$\mu 1$	−0.4655	−0.4278
ϵ_{ax}[f]	0.5475	0.2715
valence depletion CPs[g]		
ρ	0.1221	0.1475
$\nabla^2\rho$	0.1457	0.0541
α	174.1	197.4
β	53.6	36.2

[a] AIM properties in atomic units (au); angles in degrees. [b] From NBO calculations. [c] Nonbonded (3, −3) CP. [d] Radial (along bisector of ∠C1C2C3) thickness. [e] Axial thickness, ⊥ molecular plane. [f] Ellipticity in the axial plane ⊥ to the radial direction and tangential to the (3, −3) CP: $\epsilon_{ax} = (\mu 2/\mu 1) - 1$. [g] (3, +1) CPs above and below molecular plane.

TABLE 5: Diamagnetic, Paramagnetic, and Isotropic Shielding Tensors (in ppm) of C2 and Calculated and Experimental ^{13}C Chemical Shifts in Cyclopropenylidenes[a]

C2 tensors, R =	H	NMe_2
diamagnetic, σ^d	252.90	260.38
σ_{xx}^d	249.87	258.57
σ_{yy}^d	264.12	276.04
σ_{zz}^d	244.70	246.52
paramagnetic, σ^p	−327.37	−254.65
σ_{xx}^p	−678.53	−501.90
σ_{yy}^p	−323.49	−233.53
σ_{zz}^p	19.92	−28.51
isotropic, σ_{iso}	−74.47	5.73
σ_{xx}	−428.67	−243.33
σ_{yy}	−59.37	41.70
σ_{zz}	264.63	218.82
chemical shift, δ[b]	266.27	186.07
experimental shift[c] R = N(*i*-Pr)$_2$		185.51
C1(C3) tensors, R =	H	NMe_2
chemical shift, δ	191.95	154.74
experimental shift[c] R = N(*i*-Pr)$_2$		158.97

[a] See Scheme 1 for definition of axes. [b] $\delta = \sigma(\text{TMS}) - \sigma_{iso}$, where $\sigma(\text{TMS}) = 191.8$ ppm. [c] See ref 17.

effect on the nucleophilicity of the carbene carbon as a result of the amino substitution, although the radial thickness of the cap, given by the absolute value of $\mu 3$, is greater for the R = NMe_2 analogue. (A larger absolute value of $\mu 3$, the curvature of $\nabla^2\rho$ perpendicular to the surface of the cap, is indicative of a thinner radial concentration of charge.[24]) The charge concentration in the axial plane is more symmetrical for R = NMe_2, seen by the value of the ellipticity, $\epsilon_{ax} = 0.27$, as defined for this distribution by $\epsilon_{ax} = (\mu 2/\mu 1) - 1$ (see Table 4). For R = H, the axial ellipticity is larger with $\epsilon_{ax} = 0.55$.

Thus, the greater electron population of C2 realized, through in-plane σ-aromaticity, when R = NMe_2 undergoes more $\sigma-\pi$ polarization to reduce electron−electron repulsion, pushing electrons into the π-plane.[31−33]

Although due to a different mechanism, the physical properties of the topology of the electron density are consistent with the partial filling-in of the formally empty p_π* orbital on C2 as found in natural bond orbital (NBO) analysis.[52−54] As shown in Table 4, here, there is also little change in the occupancy or sp^x hybridization state of the outwardly pointing lone pair. Substantial change in the occupancy of the p_π* orbital is found, however, with p_π* containing 0.60 electrons when R = NMe_2, as compared to only 0.41 electrons when R = H. The nitrogen lone pairs participate weakly in $n_\pi(N) \rightarrow p_\pi^*(C2)$ hyperconjugation as well as strongly in $n_\pi(N) \rightarrow \pi^*(C1{=}C3)$ conjugation. The value of the second-order perturbation energy $E^{(2)}$ is 1.6 and 49.5 kcal/mol for the former and later interactions, respectively.

5. NMR Shielding Tensors and the Laplacian of the Electron Density. The magnetic properties of a molecule depend on the response of the electron density to an applied magnetic field. The shell structure of the curl of the current density ($\nabla \times J$) has been shown to mirror the map of the Laplacian of the electron density ($\nabla^2\rho$).[55,56] Thus, we can relate calculated NMR shielding tensors to the Laplacian, providing a link to an experimental method that supports our explanation of the mechanisms of stabilization.

As shown in Table 5, our calculated ^{13}C NMR chemical shifts for the R = NMe_2 model are quite close to the experimental values reported by Bertrand et al.[17] for the stable bis(diisopropylamino)cyclopropenylidene, **3**. The calculated and experimental shifts for C2 are 186.07 and 185.51 ppm, respectively, and for C1(C3), they are 154.74 and 158.97 ppm, respectively.[17]

The paramagnetic term, which admixes the ground state electron density with partially occupied or unoccupied excited states, shows the most response to changes in the valence electronic structure. The term σ_{zz}^p, for example, refers to the paramagnetic part of the shielding density due to the current induced by a magnetic field applied in the *z*-direction and is given by:[57−59]

$$\sigma_{zz}^{\,p} = -\frac{e^2\mu_0}{4\pi m_e^{\,2}} \sum_n \frac{\langle 0|l_z|n\rangle}{E_0 - E_n} \left\langle n \left| \frac{l_z}{r^3} \right| 0 \right\rangle \qquad (1)$$

where l_z is the angular momentum operator that, in a *z*-applied field, rotates density from the ground state $\langle 0|$ into the virtual state $|n\rangle$, and $E_0 - E_n$ is the energy difference between the two states. The other principal components σ_{xx}^p and σ_{yy}^p involve the l_x and l_y operators, respectively. Regions of charge depletion in the Laplacian tend to give rise to deshielding paramagnetic currents, as they contain virtual states into which orthogonal electron density may be rotated. This is evident in the σ_{xx}^p and σ_{yy}^p terms of the C2 paramagnetic tensor, which rotate the lone pair concentration (σ_{xx}^p) and σ-plane concentration (σ_{yy}^p) into the gaps in the VSCC above and below C2. For the R = H case, both terms are very deshielding, but $\sigma_{xx}^p = -678.53$ ppm is more deshielding than $\sigma_{yy}^p = -323.49$ ppm since the l_x operator rotates nonbonding concentration, of higher energy, directly into the depletion gaps. Both terms become less deshielding when R = NMe_2 due to the partial filling in of the depletion gaps by $\sigma-\pi$ polarization as discussed above.

Areas of electron concentration tend to produce shielding paramagnetic currents,[56] although the net effect of the paramagnetic term is usually deshielding. Thus, we would expect a high in-plane build-up of charge due to σ-aromaticity to produce less deshielding, or even shielding, paramagnetic currents. We find this is the case, by looking at the σ_{zz}^p term of the C2 paramagnetic tensor. When R = H, the term is actually positive, $\sigma_{zz}^p = 19.92$ ppm, as the in-plane concentrations have few unoccupied virtual states into which they can be rotated by a *z*-applied magnetic field. With R = NMe_2, there is more depletion in the ring center due to back-polarization of density into the regions along the carbon−carbon bonds, and the component $\sigma_{zz}^p = -28.51$ ppm is now slightly deshielding the C2 nucleus.

As visualization of these shielding trends, Figure 4 shows plots, in the plane of the molecules, of the isotropic shielding density of the C2 nucleus overlaid with the map of the Laplacian of the electron density. The isosurfaces show where the electron density and currents of the whole molecule in a homogeneous magnetic field are shielding (red) and deshielding (blue) the C2 nucleus. The effect of strong paramagnetic currents, due to the large perpendicular depletion gap above and below the C2 nucleus, can be easily seen. However, the in-plane build-up of density due to σ-aromaticity produces shielding currents, seen by the red isosurfaces in the bonding areas, that are only overcome by the strong deshielding near C2. Greater shielding of C2 when R = NMe_2 is seen in Figure 4b. There is less deshielding by the σ_{xx}^p and σ_{yy}^p terms to counteract the shielding currents of the σ_{zz}^p term, leading to a more shielded C2 nucleus and an upfield chemical shift of $\delta = 186.07$ ppm for **2** as compared to $\delta = 266.27$ ppm for **1**.

Finally, Figure 5 shows the shielding (red) paramagnetic currents induced by a *z*-applied magnetic field, due to the large

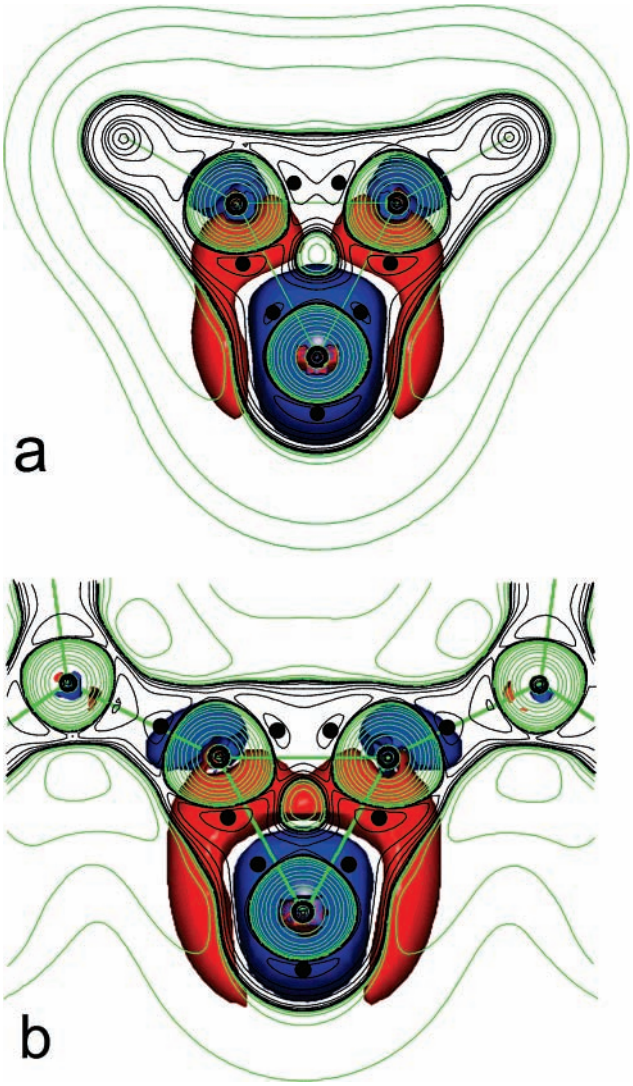

Figure 4. Isotropic shielding density of C2 in cyclopropenylidene overlaid with the map of the Laplacian of the electron density in the plane of the molecule for (a) R = H and (b) R = NMe_2. Red and blue isosurfaces show the areas where currents shield and deshield, respectively, the C2 nucleus at a value of ±1 ppm. The large deshielding due to the out-of-plane depletion gap of C2 and the shielding due to the in-plane build-up of charge due to σ-aromaticity can be easily seen.

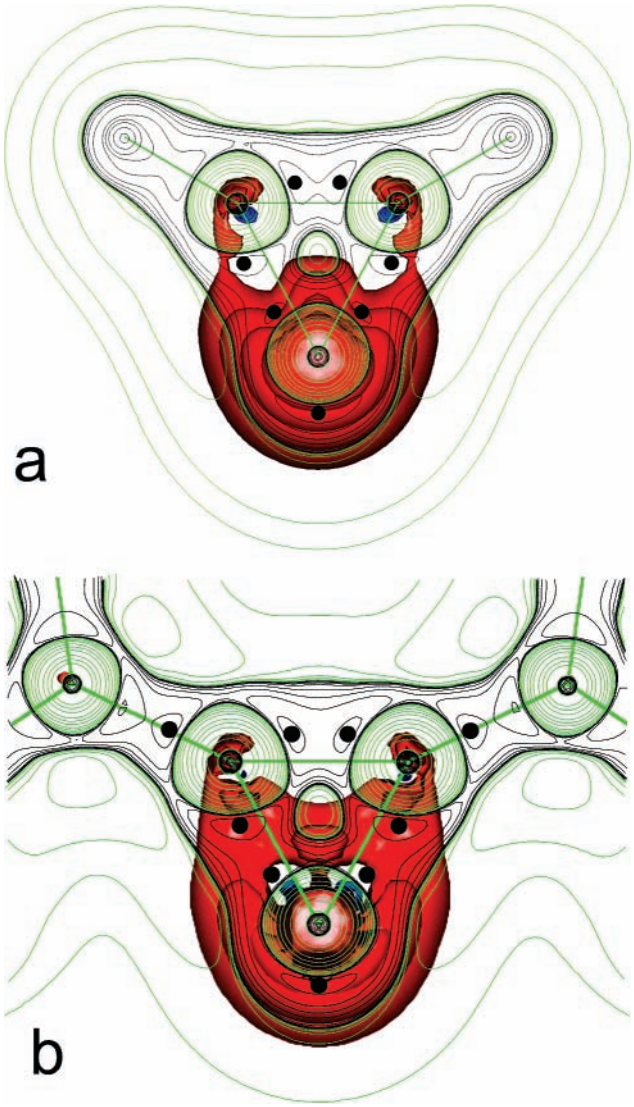

Figure 5. Isosurface of the shielding density of C2, in-plane, under a *z*-applied magnetic field, overlaid with the map of the Laplacian of the electron density in the molecular plane for (a) R = H and (b) R = NMe_2. Shielding (red) and deshielding (blue) isosurfaces are plotted at ±1 ppm.

in-plane build-up of charge due to σ-aromaticity. The effects of back-polarization when R = NMe_2 allow for some deshielding (blue) regions to encroach the shielding regions near the C2 nucleus.

IV. Conclusions

The stabilization of the normally, highly reactive carbene carbon has been traced to several mechanisms, including charge transfer, π-back-donation, π-aromaticity, and steric blocking. Using QTAIM analysis, we investigated how electronic stabilization of the C2 carbon is achieved in cyclopropenylidene by amino substitution and compared our findings to calculated and experimental NMR data. This investigation shows three sources of stabilization of C2 by nitrogen substitution in the bis(dimethylamino)cyclopropenylidene model **2** of the recently synthesized bis(diisopropylamino)cyclopropenylidene, **3**. First, as a result of charge transfer to nitrogen and subsequent back-polarization, more density is accumulated within the C2 atomic basin, thus lowering its integrated atomic energy—the hallmark of electronic stabilization of an atom. Second, the plane perpendicular lone pairs of nitrogen utilize in-plane σ-aromaticity as a conduit to delocalize charge into the C2 basin. Finally, increased π-plane concentration of charge in the valence shell of C2 is caused by $\sigma-\pi$ polarization, as opposed to π-plane back-donation as in the orbital model. This reduces the charge depletion gap above and below the plane at C2 and thus protects the carbene carbon, relative to the more reactive parent c-C_3H_2 molecule, from nucleophilic attack. This interpretation is confirmed by the nature of the asymmetry of the quadrupole tensor on the ring atoms, analysis of the ellipticity of the electron density along the BPs, and diamagnetic and paramagnetic shielding effects.

Acknowledgment. Supercomputer time allocations received from the National Computational Science Alliance and from the Advanced Biomedical Computing Center of the Frederick Cancer Research and Development Center, National Institutes of Health, are acknowledged. Support for this work also came from a Research Initiation Grant from the Office of the Vice President for Research, University of Louisville, and an Intramural Research Grant from the College of Arts and Sciences, University of Louisville. A NSF-DGE (GK-12)

graduate fellowship to L.E.J. is gratefully acknowledged. We also thank Dr. James B. Foresman for his help on procedures for the rotation and visualization of NMR shielding tensors.

Supporting Information Available: Atomic coordinates of optimized structures **1**−**3**. Complete author list for ref 36. A more detailed narrative about QTAIM methodology. This material is available free of charge via the Internet at http://pubs.acs.org.

References and Notes

(1) Thaddeus, P.; Vrtilek, J. M.; Gottlieb, C. A. *Astrophys. J.* **1985**, *299*, L63−L66.
(2) Thaddeus, P.; Gottlieb, C. A.; Mollaaghababa, R.; Vrtilek, J. M. *J. Chem. Soc. Faraday Trans.* **1993**, *89*, 2125−2129.
(3) Reisenauer, H. P.; Maier, G.; Riemann, A.; Hoffmann, R. W. *Angew. Chem., Int. Ed. Engl.* **1984**, *23*, 641.
(4) Bogey, M.; Destombes, J. L. *Astron. Astrophys.* **1986**, *159*, L8−L9.
(5) Bogey, M.; Demuynck, C.; Destombes, J. L. *Chem. Phys. Lett.* **1986**, *125*, 383−388.
(6) Bogey, M.; Demuynck, C.; Destombes, J. L.; Dubus, H. *J. Mol. Spectrosc.* **1987**, *122*, 313−324.
(7) Kanata, H.; Yamamoto, S.; Saito, S. *Chem. Phys. Lett.* **1987**, *140*, 221−224.
(8) Seburg, R. A.; Patterson, E. V.; Stanton, J. F.; McMahon, R. J. *J. Am. Chem. Soc.* **1997**, *119*, 5847−5856.
(9) Taatjes, C. A.; Klippenstein, S. J.; Hansen, N.; Miller, J. A.; Cool, T. A.; Wang, J.; Law, M. E.; Westmoreland, P. R. *Phys. Chem. Chem. Phys.* **2005**, *7*, 806−813.
(10) Maier, G.; Reisenauer, H. P.; Schwab, W.; Carsky, P.; Hess, B. A., Jr.; Schaad, L. J. *J. Am. Chem. Soc.* **1987**, *109*, 5183−5188.
(11) Maier, G.; Preiss, T.; Reisenauer, H. P.; Hess, B. A., Jr.; Schaad, L. J. *J. Am. Chem. Soc.* **1994**, *116*, 2014−2018.
(12) Maier, G.; Preiss, T.; Reisenauer, H. P. L. J. *Chem. Ber.* **1994**, *127*, 779−782.
(13) Jones, W. M.; Stowe, M. E.; Wells, E. E., Jr.; Lester, E. W. *J. Am. Chem. Soc.* **1968**, *90*, 1849−1859.
(14) DePinto, J. T.; McMahon, R. J. *J. Am. Chem. Soc.* **1993**, *115*, 12573−12574.
(15) Bourissou, D.; Guerret, O.; Gabbai, F. P.; Bertrand, G. *Chem. Rev.* **2000**, *100*, 39−91.
(16) Canac, Y.; Soleilhavoup, M.; Conejero, S.; Bertrand, G. *J. Organomet. Chem.* **2004**, *689*, 3857−3865.
(17) Lavallo, V.; Canac, Y.; Donnadieu, B.; Schoeller, W. W.; Bertrand, G. *Science* **2006**, *312*, 722−724.
(18) Phillips, E. M.; Wadamoto, M.; Chan, A.; Scheidt, K. A. *Angew. Chem., Int. Ed.* **2007**, *46*, 3107−3110.
(19) Marion, N.; Díez-González, S.; Nolan, S. P. *Angew. Chem., Int. Ed.* **2007**, *46*, 2988−3000.
(20) Schwartz, J.; Böhm, V. P. W.; Gardiner, M. G.; Grosche, M.; Herrmann, W. A.; Hieringer, W.; Raudaschl-Sieber, G. *Chem. Eur. J.* **2000**, *6*, 1773−1780.
(21) Weskamp, T.; Kohl, F. J.; Hieringer, W.; Gleich, D.; Herrmann, W. A. *Angew. Chem., Int. Ed.* **1999**, *38*, 2416−2419.
(22) Culkin, D. A.; Jeong, W.; Csihony, S.; Gomez, E. D.; Balsara, N. P.; Hendrick, J. L.; Waymouth, R. M. *Angew. Chem., Int. Ed.* **2007**, *46*, 2627−2630.
(23) Frey, G. D.; Lavallo, V.; Donnadieu, B.; Schoeller, W. W.; Bertrand, G. *Science* **2007**, *316*, 439−441.
(24) Bader, R. F. W. *Atoms in Molecules. A Quantum Theory*; Clarendon Press: Oxford, 1990.
(25) Popelier, P. *Atoms in Molecules. An Introduction*; Prentice Hall: New York, 2000.
(26) MacDougall, P. J.; Bader, R. F. W. *Can. J. Chem.* **1986**, *64*, 1496−1508.
(27) Dewar, M. J. S. *J. Am. Chem. Soc.* **1984**, *106*, 669−682.
(28) Cremer, D. *Tetrahedron* **1988**, *44*, 7427−7453.
(29) Cremer, D.; Kraka, E. *J. Am. Chem. Soc.* **1985**, *107*, 3800−3810.
(30) Cremer, D.; Gauss, J. *J. Am. Chem. Soc.* **1986**, *108*, 7467−7477.
(31) Wiberg, K. B.; Hadad, C. M.; Breneman, C. M.; Laidig, K. E.; Murcko, M. A.; LePage, T. J. *Science* **1991**, *252*, 1266−1272.
(32) Bader, R. F. W.; Chang, C. *J. Phys. Chem.* **1989**, *93*, 5095−5107.
(33) Wiberg, K. B.; Rosenberg, R. E.; Rablen, P. R. *J. Am. Chem. Soc.* **1991**, *113*, 2890−2898.
(34) Becke, A. D. *J. Chem. Phys.* **1993**, *98*, 5648−5652.
(35) Lee, C.; Yang, W.; Parr, R. G. *Phys. Rev.* **1988**, *B37*, 785−789.
(36) Frisch, M. J.; et al. *Gaussian03*, Revision C.02; Gaussian, Inc.: Wallingford, CT, 2004.
(37) Biegler-Konig, F.; Schonbohm, J. *J. Comput. Chem.* **2002**, *23*, 1489−1494.
(38) Fradera, X.; Austen, M. A.; Bader, R. F. W. *J. Phys. Chem. A* **1999**, *103*, 304−314.
(39) Ditchfield, R. *Mol. Phys.* **1974**, *27*, 789−807.
(40) Wolinksi, K.; Hinton, J. F.; Pulay, P. *J. Am. Chem. Soc.* **1990**, *112*, 8251−8260.
(41) Kovács, J.; Tóth, G.; Simon, A.; Lévai, A.; Koch, A.; Kleinpeter, E. *Magn. Reson. Chem.* **2003**, *41*, 193−201.
(42) Vázquez, S. *J. Chem. Soc., Perkin Trans. 2* **2002**, *2*, 2100−2103.
(43) Dobado, J. A.; Benkadour, N.; Melchor, S.; Portal, D. *J. Mol. Struct. (Theochem)* **2004**, *672*, 127−132 and references within.
(44) Laaksonen, L. *J. Mol. Graph.* **1992**, *10*, 33−34.
(45) Bergman, D. L.; Laaksonen, L.; Laaksonen, A. *J. Mol. Graphics Modell.* **1997**, *15*, 301−306.
(46) Wiberg, K. B.; Bader, R. F. W.; Lau, C. D. H. *J. Am. Chem. Soc.* **1987**, *109*, 985−1001.
(47) Bader, R. F. W.; MacDougall, P. J.; Lau, C. D. H. *J. Am. Chem. Soc.* **1984**, *106*, 1594−1605.
(48) Bader, R. F. W.; Slee, T. S.; Cremer, D.; Kraka, E. *J. Am. Chem. Soc.* **1983**, *105*, 5061−5068.
(49) Cheeseman, J. R.; Carroll, M. T.; Bader, R. F. W. *Chem. Phys. Lett.* **1988**, *143*, 450−458.
(50) Tafipolsky, M.; Scherer, W.; Ofele, K.; Artus, G.; Pedersen, B.; Herrmann, W. A.; McGrady, G. S. *J. Am. Chem. Soc.* **2002**, *124*, 5865−5880.
(51) Gatti, C.; MacDougall, P. J.; Bader, R. F. W. *J. Chem. Phys.* **1988**, *88*, 3782−3804.
(52) Glendening, E. D.; Badenhoop, J. K.; Reed, A. E.; Carpenter, J. E.; Bohmann, J. A.; Morales, C. M.; Weinhold, F. *NBO 5.0 Program Manual. Natural Bond Orbital Analysis Programs*, NBO 5.0; Theoretical Chemistry Institute, University of Wisconsin: Madison, WI, 2001.
(53) Reed, A. E.; Curtiss, L. A.; Weinhold, F. *Chem. Rev.* **1988**, *88*, 899−926.
(54) Weinhold, F. Natural bond orbital methods. In *The Encyclopedia of Computational Chemistry*; Schleyer, P. v. R., Ed.; John Wiley & Sons: Chichester, 1998.
(55) Keith, T. A.; Bader, R. F. W. *J. Chem. Phys.* **1993**, *99*, 3669−3682.
(56) Bader, R. F. W.; Keith, T. A. *J. Chem. Phys.* **1993**, *99*, 3683−3693.
(57) Wiberg, K. B.; Hammer, J. D.; Zilm, K. W.; Cheeseman, J. R.; Keith, T. A. *J. Phys. Chem. A* **1998**, *102*, 8766−8773.
(58) Wiberg, K. B.; Hammer, J. D.; Keith, T. A.; Zilm, K. W. *J. Phys. Chem. A* **1999**, *103*, 21−27.
(59) Ramsey, N. F. *Phys. Rev.* **1950**, *78*, 699−703.